

Estimates of micro-, nano-, and picoplankton contributions to particle export in the northeast Pacific

B. L. Mackinson¹, S. B. Moran¹, M. W. Lomas², G. M. Stewart³, R. P. Kelly¹

[1] {Graduate School of Oceanography, University of Rhode Island, Narragansett, RI 02882, USA}

[2] {Bigelow Laboratory for Ocean Sciences, East Boothbay, ME 04544, USA}

[3] {Queens College and Graduate Center, City University of New York, Flushing, NY 11367, USA}

Correspondence to: B. L. Mackinson (bmackinson@my.uri.edu)

Abstract

The contributions of micro-, nano-, and picoplankton to particle export were estimated from measurements of size-fractionated particulate ^{234}Th , organic carbon, and phytoplankton indicator pigments obtained during five cruises between 2010 and 2012 along Line P in the subarctic northeast Pacific Ocean. Sinking fluxes of particulate organic carbon (POC) and indicator pigments were calculated from ^{234}Th – ^{238}U disequilibria and, during two cruises, measured by sediment trap at Ocean Station Papa. POC fluxes at 100 m ranged from 0.65 – 7.95 $\text{mmol m}^{-2} \text{d}^{-1}$, similar in magnitude to previous results at Line P. Microplankton pigments dominate indicator pigment fluxes (averaging $69 \pm 19\%$ of total pigment flux), while nanoplankton pigments comprised the majority of pigment standing stocks (averaging $64 \pm 23\%$ of total pigment standing stock). Indicator pigment loss rates (the ratio of pigment export flux to pigment standing stock) point to preferential export of larger microplankton relative to smaller nano- and picoplankton. However, indicator pigments do not quantitatively trace particle export resulting from zooplankton grazing, which may be an important pathway for the export of small phytoplankton. These results have important implications for understanding the magnitude and

31 mechanisms controlling the biological pump at Line P in particular, and more generally in
32 oligotrophic gyres and high-nutrient, low-chlorophyll regions where small phytoplankton
33 represent a major component of the autotrophic community.

34

35 **1 Introduction**

36 Phytoplankton community structure exerts an important influence on the strength and
37 efficiency of the biological pump (Michaels and Silver, 1988; Boyd and Newton, 1999; Thibault
38 et al., 1999; Brew et al., 2009; Lomas and Moran, 2011). Small nano- and picoplankton
39 dominate the phytoplankton community in the oligotrophic gyres and high-nutrient, low-
40 chlorophyll (HNLC) oceanographic regions. It has traditionally been thought that small
41 phytoplankton represent a relatively small fraction of the downward flux of particulate organic
42 carbon (POC) relative to larger phytoplankton, such as diatoms, which are generally thought to
43 contribute disproportionately to POC export (e.g., Michaels and Silver, 1988). Recent studies
44 have challenged this idea, suggesting that small phytoplankton contribute significantly to POC
45 export, possibly through aggregation and incorporation into fecal pellets (Richardson and
46 Jackson, 2007; Amacher et al., 2009; Stukel and Landry, 2010; Lomas and Moran, 2011; Stukel
47 et al., 2013). A better understanding of the controls on the relative importance of small
48 phytoplankton in POC export is needed to refine our understanding of the magnitude and
49 mechanisms controlling the biological pump, particularly as recent climate models predict an
50 expansion of the oligotrophic gyres where small cells dominate (Irwin et al., 2006; Polovina et
51 al., 2008; Morán et al., 2010).

52 Ocean Station Papa (OSP, 50°N, 145°W), the site of one of the longest-running ocean
53 time-series, is located in the northeast Pacific Ocean in one of three major HNLC regions.
54 Previous attempts to resolve the apparent paradox of low phytoplankton biomass and high nitrate
55 concentrations at OSP concluded that a bottom-up control related to iron limitation is most
56 important for large phytoplankton (Muggli et al., 1996; Harrison, 2006; Marchetti et al., 2006),
57 while microzooplankton grazing exerts a strong top-down control on pico- and nanoplankton
58 (Landry et al., 1993; Harrison et al., 1999; Rivkin et al., 1999). Primary production at the
59 stations proximal to the coast on Line P (P4 & P12) is not iron-limited and diatom blooms are
60 typically observed in spring and late summer (Boyd and Harrison, 1999; Thibault et al., 1999).
61 At the offshore stations (including OSP) the phytoplankton community is dominated by cells <5-

62 μm and the seasonal variability of primary production is relatively low ($\sim 25 \text{ mmol C m}^{-2} \text{ d}^{-1}$ in
63 winter and $\sim 67 \text{ mmol C m}^{-2} \text{ d}^{-1}$ in summer) (Boyd and Harrison, 1999; Thibault et al., 1999;
64 Choi et al., 2014). In contrast to the low variability in primary production, POC export recorded
65 by moored sediment traps at OSP exhibits a stronger seasonal cycle with fluxes at 200 m depth
66 ranging from $\sim 0.4 \text{ mmol C m}^{-2} \text{ d}^{-1}$ in winter to $\sim 2.4 \text{ mmol C m}^{-2} \text{ d}^{-1}$ in summer (Timothy et al.,
67 2013). The average annual sediment trap POC flux at OSP ($1.4 \pm 1.1 \text{ mmol C m}^{-2} \text{ d}^{-1}$) is nearly
68 five times lower than the annual net community production (ANCP) at OSP ($6.3 \pm 1.6 \text{ mmol C}$
69 $\text{m}^{-2} \text{ d}^{-1}$), suggesting that the majority of organic carbon export is due to active transport by
70 zooplankton and/or dissolved organic carbon (DOC) export (Timothy et al., 2013; Emerson,
71 2014).

72 This study builds upon prior investigations of phytoplankton community composition and
73 export production along Line P by examining the distributions of organic carbon, phytoplankton
74 indicator pigments, and ^{234}Th in three particle size-fractions. Sinking fluxes of POC and
75 indicator pigments from the upper waters ($\sim 100 \text{ m}$) were calculated from the ^{234}Th – ^{238}U
76 disequilibrium and, during two cruises, measured at OSP using free-floating sediment traps. A
77 comparison of indicator pigment fluxes with the respective standing stocks suggests that
78 microplankton ($20 - 200\text{-}\mu\text{m}$) make up a higher percentage of particle export than biomass,
79 whereas pico- and nano plankton ($0.2 - 2\text{-}\mu\text{m}$ and $2 - 20\text{-}\mu\text{m}$) make up a lower percentage of
80 particle export than biomass.

81

82 2 Methods

83 2.1 Study location

84 Sample collection was conducted at five stations along Line P (P4, P12, P16, P20, and
85 P26 (OSP)) during cruises aboard the *CCGS John P. Tully* in August 2010, February 2011, June
86 2011, February 2012, and June 2012 (Fig. 1, Table 2). Line P is located at the southern edge of
87 the Alaskan Gyre, and the prevailing winds and surface currents are west-east (Bograd et al.,
88 1999). Because precipitation and continental run-off exceed evaporation, a permanent halocline
89 exists at $\sim 100 \text{ m}$ impeding deep winter mixing. In addition, a seasonal thermocline forms at ~ 50
90 m in spring and shoals to $\sim 20 \text{ m}$ in summer (Freeland et al., 1997; Thibault et al., 1999;
91 Freeland, 2013; Timothy et al., 2013).

92

94 2.2 Net primary production by ^{14}C incubation

95 Rates of net primary production (NPP) were determined following the protocols outlined
96 in Lomas et al. (2012). Samples were collected with Niskin bottles from seven depths in the
97 euphotic zone corresponding to 1, 5, 9, 17, 33, 55, and 100% of surface irradiance. Three ‘light’
98 bottles, a single ‘dark’ bottle, and a single initial (T_0) bottle were each spiked with $\sim 10\ \mu\text{Ci}$
99 $\text{NaH}^{14}\text{CO}_3$. A sub-sample to confirm total added activity was removed from the T_0 bottle at each
100 light depth and immediately added to an equal volume of β -phenylethylamine. Bottles were
101 incubated under simulated in situ conditions, using neutral density screening to mimic light
102 levels at the depth of sample collection, in an on-deck incubator for ~ 24 hours. After incubation,
103 125 mL sub-samples from each light and dark bottle were filtered through an Ahlstrom 151 (0.7-
104 μm nominal pore size) and a Whatman Track Etch 5- μm filter and rinsed with 10% HCl.
105 Samples were counted on a Perkin Elmer TriCarb 2900LR ~ 48 h after the addition of 5 mL of
106 Ultima Gold (Perkin Elmer, USA) scintillation cocktail.

108 2.3 Water column ^{234}Th

109 Total ^{234}Th (dissolved + particulate) analysis followed the procedures outlined in Bauman
110 et al. (2013). Briefly, samples (4 L) were collected by Niskin bottle at 12 depths (surface to
111 ~ 500 m) and spiked with ^{230}Th to monitor Th recovery. Samples were then treated with 7-8
112 drops of concentrated NH_4OH solution, followed by 25 μL of 0.2 M KMnO_4 , and finally with
113 11.5 μL of 1.0 M MnCl_2 to form a MnO_2 precipitate that quantitatively scavenges Th (Benitez-
114 Nelson et al., 2001; Buesseler et al., 2001; van der Loeff et al., 2006). After 1 hour, samples
115 were vacuum filtered onto 25 mm glass microfiber filters (GM/F, 1- μm nominal pore size) that
116 were frozen for later analysis in the shore-based laboratory. To prepare samples for counting,
117 filters were dried at 50°C for ~ 24 hours, mounted on acrylic planchets, and covered with
118 aluminum foil. To quantify ^{234}Th , the beta emission of $^{234\text{m}}\text{Pa}$ ($E_{\text{max}} = 2.19\ \text{MeV}$; $t_{1/2} = 1.2\ \text{min}$)
119 was counted using a RISØ National Laboratory low-background beta detector (Roskilde,
120 Denmark). Each sample was counted four times over a period of approximately six half-lives,
121 with the first count made at least 10 days after collection to allow for the decay of short-lived
122 isotopes, and the final count used to quantify background levels. Data were fitted to the ^{234}Th
123 decay curve to calculate the decay-corrected activity at the time of sample collection. Following
124 the ^{234}Th analysis, Th was radiochemically purified and ^{230}Th was measured by alpha particle

emission in order to determine scavenging efficiency. Small-volume scavenging efficiencies were found to be >90%. ^{238}U activities were calculated from salinity using the relationship $^{238}\text{U} = 0.07081 \times S$ (‰) (Chen et al., 1986)

2.4 Water column POC, Chl *a*, and indicator pigments

Water samples for POC, Chl *a*, and phytoplankton indicator pigments were collected from the same depths in the photic zone as for NPP samples. Suspended POC was measured on 1 L seawater samples filtered onto pre-combusted Ahlstrom 151 filters and frozen at -20°C until analysis. Samples were dried at 60°C in a drying oven, fumed in a desiccator containing concentrated hydrochloric acid for 24 h to remove inorganic carbonates, and dried again at 60°C. Samples were then analyzed on an EA-440 Analyzer (Exeter Analytical, Inc., Chelmsford, MA). Chl *a* samples were analyzed using the methods outlined in Lomas et al. (2012). Separate samples (~0.2 L) were filtered onto Ahlstrom 151 and 5-μm Whatman Track Etch polycarbonate filters and frozen at -20°C until analysis. Samples were then extracted in 5 mL of 90% acetone for 24 h at -20°C and analyzed using a calibrated TD-700 fluorometer.

Indicator pigment samples were collected on separate Ahlstrom 151 filters and stored at -80°C until analysis by high-performance liquid chromatography (HPLC) at the Bermuda Institute of Ocean Sciences in the Bermuda Atlantic Time-series Study Laboratory (Knap et al., 1997). Fucoxanthin (FUCO), peridinin (PER), 19'-hexanoyloxyfucoxanthin (HEX), 19'-butanoyloxyfucoxanthin (BUT), alloxanthin (ALLO), total chlorophyll *b* (TChl *b*), and zeaxanthin (ZEA) were analyzed as indicator pigments based on their correspondence to particular phytoplankton taxonomic groups. Indicator pigment proportion factors (PFs) were calculated to further analyze the size-distribution of the phytoplankton community (Hooker et al., 2005; Lomas and Moran, 2011). The sum of FUCO and PER concentrations was used to determine the microplankton proportion factor (mPF), while the sum of HEX, BUT, ALLO, and TChl *b* was used to determine the nanoplankton proportion factor (nPF), and ZEA was used to determine the picoplankton proportion factor (pPF) (Hooker et al., 2005; Lomas and Moran, 2011). Hooker et al. (2005) included TChl *b* in pPF, but because *Prochlorococcus* is not found in the study region, it was assumed in this study that any Chl *b* would be found in cells (e.g., chlorophytes and euglenophytes) in the nanoplankton size-class.

2.5 In situ pump sampling

Large-volume in situ pumps (Challenger Oceanic Systems and Services, UK and McLane Scientific, Falmouth, MA) were deployed for approximately four hours at depths of 30, 50, 100, 150, and 200 m. Each pump sampled 100 – 1000 liters to collect size-fractionated particles, with seawater passing sequentially through 53- μ m, 10- μ m, and 1- μ m Nitex screens. Particles were resuspended by ultrasonication in 0.7- μ m prefiltered seawater and filtered onto separate pre-combusted GF/F filters for parallel analysis. Indicator pigment samples were stored at -80°C until analysis by high-performance liquid chromatography (HPLC) at the Bermuda Institute of Ocean Sciences in the Bermuda Atlantic Time-series Study Laboratory (Knap et al., 1997). Filters for analysis of POC and ^{234}Th were frozen at -20°C until analysis. A sub-sample (~30% by weight) was cut with acetone-cleaned stainless steel scissors from each ^{234}Th filter for POC analysis, and these sub-samples were dried and fumed with concentrated HCl as described above. POC was then measured using a CE 440 CHN Elemental Analyzer (Exeter Analytical, Inc., Chelmsford, MA). The ^{234}Th filter subsample was dried at 60°C in a drying oven and counted on a RISØ beta detector as noted above.

2.6 Sediment trap sampling

Surface-tethered particle interceptor traps (PITS) with cylindrical tubes (KC-Denmark, Silkeborg, Denmark) were deployed for ~3 days at station P26 during the June 2011 and June 2012 cruises to collect particles at the depths of 30, 50, 100, 150, and 200 m. Due to limited wire-time and other cruise constraints it was not possible to deploy sediment traps at any other stations sampled as part of this study. The trap design and sampling procedure is described in Baumann et al. (2012). Four tubes (72 mm diameter, 450 mm length) were used at each depth, and tubes were filled with non-poisoned, 0.4- μ m filtered brine ($S = \sim 85 \text{ ‰}$) prior to deployment. Upon recovery trap brines were combined, particles were re-suspended and filtered onto pre-combusted GF/F filters, and swimmers were removed. Filters were stored frozen and later analyzed for POC, ^{234}Th , and indicator pigments as described above.

3 Results

3.1 Hydrography and NPP

186 Depth sections of temperature and density anomaly (σ_t) were generated using
187 results from all CTD casts for a given cruise to improve horizontal data resolution (Fig. 2). The
188 seasonal change in water temperature is largely confined to the upper ~100 m. Surface
189 temperatures in August 2010 were ~14°C, while during the February cruises, surface
190 temperatures were slightly cooler offshore (~6°C) than inshore (~8°C). During the June cruises,
191 inshore temperatures were warmer (~10 – 12°C) while offshore temperatures remained relatively
192 cool (~8°C). Density anomaly did not vary greatly between cruises below ~100 m. During the
193 winter, a pool of less dense water (density of 1023 – 1025 kg m⁻³) was observed toward the coast
194 (east of ~126°W). During the June cruises, this pool was observed extending west to ~130°W
195 and during August 2010, it extended out to OSP (145°W). These data follow the expected
196 seasonal pattern of a well-mixed water column in winter and increasing stratification moving
197 from spring to summer.

198 Total NPP and >5- μ m size-fractionated NPP values were trapezoidally integrated over
199 the euphotic zone (Table 3). A maximum total NPP of 91.9 mmol m⁻² d⁻¹ was measured at
200 station P26 during June 2011, whereas the lowest value of 23.4 mmol m⁻² d⁻¹ was measured at
201 station P26 during February 2012. These values agree to within a factor of two with the seasonal
202 averages reported by Boyd and Harrison (1999). A maximum >5- μ m NPP of 39.6 mmol m⁻² d⁻¹
203 was at station P4 during June 2012 and a minimum of 3.2 mmol m⁻² d⁻¹ was measured at station
204 P20 in February 2011.

206 3.2 Small- and large-volume POC concentrations

207 Suspended POC concentrations from Niskin bottle samples collected in the photic zone
208 range from 1.1 – 7.1 μ mol L⁻¹. POC concentrations were generally lowest at the base of the
209 photic zone, though decreasing concentrations with depth were not observed at all stations (Table
210 S1). The highest suspended POC concentrations were measured at station P4 during all cruises.
211 POC concentrations were also measured in three size-fractions of particles collected with large-
212 volume in situ pumps (Table S2). Concentrations of each size-fraction tended to decrease with
213 depth and were typically less than 0.5 μ mol L⁻¹ at all depths. One exception was at station P26
214 during February 2011 when POC concentrations at 30 m were between 1.8 and 2.9 μ mol L⁻¹ for
215 all size-fractions.

Brendan Mackinson 4/2/2015 9:29 PM

Deleted: 2

Brendan Mackinson 4/7/2015 12:49 AM

Deleted: 1

Brendan Mackinson 4/7/2015 12:50 AM

Deleted: 2

Brendan Mackinson 4/7/2015 12:50 AM

Deleted: 1

Brendan Mackinson 4/7/2015 12:50 AM

Deleted: 2

221 The concentrations of POC collected using small-volume and large-volume methods
 222 often do not agree for samples collected at the same location and depth (Gardner, 1977; Moran et
 223 al., 1999; Liu et al., 2005; Liu et al., 2009). As reported in these previous studies, POC
 224 concentrations measured by large-volume in situ pumps (summed for all size-fractions) are
 225 significantly (ANOVA, $p < 0.05$) less than small-volume POC measurements from the same
 226 station and similar depth (Fig. 3a). Explanations put forth to account for this discrepancy include
 227 DOC adsorption to filters, pressure effects on particle retention in pump samples, the collection
 228 of zooplankton by Niskin bottles but not pumps, and particle washout from pump filters (Moran
 229 et al., 1999; Liu et al., 2005; Liu et al., 2009). In this study, the smallest pump size-fraction
 230 was collected using a 1- μm Nitex screen, not a GF/F, resulting in the pumps missing the portion
 231 of the POC on particles between 0.7- and 1- μm , which may further contribute to the difference
 232 observed between the two methods. Lomas and Moran (2011) reported that sonication of in situ
 233 pump samples to resuspend particles from the Nitex screens had no significant effect on
 234 measured POC concentrations.

235

236 3.3 Particulate ^{234}Th and $\text{POC}/^{234}\text{Th}$ ratios

237 Size-fractionated particulate ^{234}Th activities in samples collected by in situ pump
 238 generally decrease with depth, and are typically less than 0.1 dpm L^{-1} (Table S2). As with in situ
 239 pump POC concentrations, station P26 during February 2011 is an exception, with values
 240 exceeding 0.1 dpm L^{-1} for all size fractions at 30 m and throughout most of the water column for
 241 the 1 – 10- μm fraction. Size-fractionated $\text{POC}/^{234}\text{Th}$ ratios (Fig. 4a, Table S2) are less than ~ 6
 242 $\mu\text{mol dpm}^{-1}$ for all size-classes at most stations, with higher values measured at stations P4 and
 243 P12 in February 2012 and P4 in June 2012. $\text{POC}/^{234}\text{Th}$ ratios tend to decrease or remain constant
 244 with depth, with one exception at station P12 during February 2012 where the maximum
 245 $\text{POC}/^{234}\text{Th}$ was at 100 m for all size fractions. Also, the $\text{POC}/^{234}\text{Th}$ ratio does not vary greatly
 246 between size-fractions (Fig. 4a) as was observed in Speicher et al. (2006) and Brew et al. (2009).

247 The accuracy of ^{234}Th as a tracer of POC export depends on the assumption that ^{234}Th
 248 and POC are sinking on the same particles, and therefore sinking at the same rate (Moran et al.,
 249 2003; Smith et al., 2006; Speicher et al., 2006; Burd et al., 2007; Brew et al., 2009). A high
 250 degree of correlation between the size-fractionated distributions of ^{234}Th and POC (Fig. 4b-d)
 251 along Line P provides evidence in support of this assumption. All correlations were statistically

significant ($p < 0.05$) and imply a strong coupling between particulate ^{234}Th and POC for all cruises. In addition, the clustering of data for the different size-fractions of particles (Fig. 4) indicates that in February 2012 the 10 – 53- μm size class contained the highest percentage of POC and particulate ^{234}Th , while the >53- μm size class contained the lowest percentage. In June 2012, the 1 – 10- μm size class had the lowest percentage of POC and particulate ^{234}Th while both the 10 – 53- μm and the >53- μm fractions contained higher percentages (Fig. 4b-d).

3.4 Small-volume Chl *a* and indicator pigments

Concentrations of total Chl *a* and >5- μm Chl *a* measured by fluorometer (Table S1) were trapezoidally integrated over the photic zone to determine respective standing stocks. During August 2010, the >5- μm fraction accounted for >30% of the Chl *a* at all stations, with a maximum of 50% at station P26. During the other four cruises, the >5- μm size-fraction generally accounted for <30% of the total Chl *a*, except at station P26 in February 2012 and station P4 in June 2012. Previous studies have reported that larger cells are more abundant at stations closer to the coast (Boyd and Harrison, 1999), though this was not always apparent. The highest >5- μm percentage of Chl *a* was measured at station P26 during August 2010, June 2011, and February 2012. Phytoplankton indicator pigments and Chl *a* concentrations in samples from the euphotic zone samples were also measured by HPLC (Table S1). HPLC and fluorescence Chl *a* concentrations generally agreed to within a factor of two, and the correlation between the two measurements was statistically significant ($p < 0.05$) (Fig. S1). The correlation between the sum of the indicator pigment concentrations and the Chl *a* concentration was statistically significant ($p < 0.05$) and roughly 1:1, suggesting that the indicator pigments examined in this analysis accounted for most of the phytoplankton biomass (Fig. S2). Furthermore, the correlation between the >5- μm fraction of Chl *a* and mPF is statistically significant ($p < 0.05$), suggesting that this PF is a reasonable representation of that size-fraction of the phytoplankton community. Profiles of indicator pigment concentrations were trapezoidally integrated over the photic zone to quantify standing stocks (Table 4). FUCO was the most abundant microplankton pigment, and HEX was the most abundant nanoplankton pigment at most stations. Indicator pigment PFs (Fig. 5, Table S3) reveal that the phytoplankton community was typically dominated by nanoplankton, although at P4, and to a lesser extent at P20 in June 2012, microplankton pigments made up the bulk of the sample (~86% and ~52% respectively).

Brendan Mackinson 4/2/2015 9:27 PM
Deleted: 3

284

285 3.5 Large-volume size-fractionated Chl *a* and indicator pigments

286 Size-fractionated Chl *a* and indicator pigment concentrations were also measured by in
287 situ pump (Table S4). Chl *a* was once again strongly correlated in a roughly 1:1 ratio with the
288 sum of the indicator pigments ($p < 0.05$) (Fig. S3). The highest Chl *a* concentrations were
289 measured in the 10 – 53- μm fraction during all cruises. In February 2012, the >53- μm fraction
290 generally had the lowest concentrations, while in June 2012 and June 2011 the lowest
291 concentrations were generally in the 1 – 10- μm fraction.

292 Ideally, small-volume and large-volume concentrations of Chl *a* and indicator pigments
293 should agree for samples collected at the same station and depth, but this was not observed in
294 this study (Fig. 3). Although differences between small- and large-volume measurements of
295 POC have been reported (Gardner, 1977; Moran et al., 1999; Liu et al., 2005; Liu et al., 2009),
296 few studies have compared Niskin bottle and in situ pump measurements of indicator pigments
297 (Lomas and Moran, 2011). Relative to bottle samples, the pump samples indicate higher
298 concentrations of microplankton pigments FUCO and PER and lower concentrations of ZEA and
299 TChl *b*, which are pigments associated with pico- and nanoplankton (Fig. 3b-d). Large-volume
300 pump and small-volume bottle measurements of the nanoplankton indicator pigments HEX,
301 BUT, and ALLO generally agree within a factor of two (Fig. 3b-d). Given the small size of
302 ZEA-containing *Synechococcus* and TChl *b*-containing chlorophytes and prasinophytes, it is
303 likely that many of these cells pass through the 1- μm Nitex screen which would lead to under-
304 sampling by the pumps (Liu et al., 2005). Bottles may undersample large, rare cells because the
305 small volume might not be a statistically representative sample (Lomas and Moran, 2011).
306 Furthermore, larger cells may settle below the spigot of the Niskin bottles, leading to a further
307 bias against the collection of large cells (Gardner, 1977; Gundersen et al., 2001). Pumps sample
308 higher concentrations of Chl *a* than bottles (Fig. 3a) at stations with high concentrations of Chl *a*,
309 but when Chl *a* concentrations are low ($<200 \text{ ng L}^{-1}$), the pumps tend to undersample relative to
310 the bottles.

311 Given these sampling differences, it is important to note that although the total
312 concentrations (summed for all size-fractions) measured by the in situ pumps may be inaccurate,
313 it is still possible that the >53- μm fraction accurately represents the composition of sinking
314 particles. The disruption of loosely-bound aggregates during collection by the pumps could

cause an error in the >53- μm fraction, but this is considered unlikely due to the presence of nanoplankton (and in some cases picoplankton) pigments in this fraction. Furthermore, a recent study in the Sargasso Sea employed a similar methodology and also found picoplankton pigments in three particle size-classes, each >10- μm (Lomas and Moran, 2011).

Indicator pigment PFs calculated for the size-fractionated particles (Table S3) and plotted against depth (Figs. 6-8) reveal that while the overall indicator pigment concentrations vary with depth and across size-fractions, the PFs do not exhibit a systematic pattern of variation across size classes, depths, or seasons. The picoplankton pigment ZEA typically represents <10% of the total indicator pigments for all size classes. Microplankton pigments dominated samples at station P4 in February 2012 and June 2012, with mPFs typically exceeding 0.5 and 0.8, respectively, for each cruise. In addition, mPFs were high at station P26 during these times, with values generally exceeding 0.5 (Figs. 7-8). Nanoplankton pigments dominated at station P12 in February 2012 cruise with nPFs exceeding 0.5 for most samples. As with the small volume samples, FUCO was usually the most abundant microplankton pigment while HEX was usually the most abundant nanoplankton pigment (Table S4).

3.6 Total ^{234}Th , $^{234}\text{Th}/^{238}\text{U}$ activity ratios, and ^{234}Th fluxes

Total (dissolved + particulate) ^{234}Th activities, ^{238}U activities, and $^{234}\text{Th}/^{238}\text{U}$ activity ratios are listed in Table S5. Depth sections of these $^{234}\text{Th}/^{238}\text{U}$ activity ratios (Fig. 2d) indicate that areas of low $^{234}\text{Th}/^{238}\text{U}$ are prevalent in spring and summer and corresponding to periods known to have high particle export in this region (Wong et al., 1999; Timothy et al., 2013). ^{234}Th fluxes (P_{Th}) were calculated using these $^{234}\text{Th}/^{238}\text{U}$ results and a 2-D steady-state model of the radiochemical balance for ^{234}Th in the upper ocean,

$$\frac{\partial A_{Th}}{\partial t} = A_U \lambda_{Th} - A_{Th} \lambda_{Th} - P_{Th} + K_h \frac{\partial^2 A_{Th}}{\partial^2 x} + U_h \frac{\partial A_{Th}}{\partial x} \quad (1)$$

where A_U is the activity of ^{238}U , λ_{Th} is the ^{234}Th decay constant, A_{Th} is the activity of ^{234}Th , P_{Th} is the vertical flux of ^{234}Th on sinking particles, K_h is the eddy diffusion coefficient, and U_h is the current velocity (Coale and Bruland, 1985; Charette et al., 1999). Assuming a steady-state

($\partial A_{Th}/\partial t = 0$) over several weeks to months, and that the diffusive flux of ^{234}Th is small relative to advection and can therefore be ignored, the vertical flux of ^{234}Th (in $\text{dpm m}^{-2} \text{d}^{-1}$) is defined by,

$$P_{Th} = \int_0^z \left[\lambda_{Th} (A_U - A_{Th}) + U_h \frac{\partial A_{Th}}{\partial x} \right] dz \quad (2)$$

where z is the depth of the water column over which the flux is measured. In this study, the gradient of thorium ($\partial A_{Th}/\partial x$) was only measured in the east-west direction (along Line P). Therefore, x is the east-west distance across which the gradient will be measured and U_h is the east-west current velocity. Current velocities determined from 5-year seasonal averages of surface drifter data (available from Fisheries and Oceans Canada) were found to be $6 \pm 4 \text{ cm s}^{-1}$ for the February cruises, $4 \pm 2 \text{ cm s}^{-1}$ for the June cruises, and $5 \pm 3 \text{ cm s}^{-1}$ for the August cruise. These values agree well with the $\sim 10 \text{ cm s}^{-1}$ value reported by McNally, (1981) and used by Charette et al., (1999). Given that the currents in the region generally flow west-east, and with no data at stations north and south of Line P, the north-south transport of ^{234}Th by advection had to be assumed to be negligible. At stations P12, P16, and P20, the ^{234}Th gradient was measured between the adjacent stations. For stations P4 and P26 (at either end of Line P), the gradient of ^{234}Th was determined from the adjacent station assuming a linear change extended beyond the measured transect.

^{234}Th fluxes (P_{Th}) calculated using the 2-D model are within 5% of fluxes determined using a steady-state 1-D model that ignores advection (Fig. S4). This indicates that, under these assumptions, the vertical flux of ^{234}Th on sinking particles is the dominant transport term. Consistent with previous studies, ^{234}Th fluxes at all stations were higher during the August and June cruises than during the February cruises (Fig. 9a) (Charette et al., 1999). Also, ^{234}Th fluxes did not exhibit a consistent trend along Line P.

3.7 ^{234}Th -derived POC fluxes

The $\text{POC}/^{234}\text{Th}$ ratio in the $>53\text{-}\mu\text{m}$ size-class and P_{Th} for a given depth horizon were used to calculate POC fluxes (P_{POC}) (Fig. 9). In most cases, P_{POC} decreases with depth, although in some cases, the maximum P_{POC} in a given profile occurs at 50 or 100 m. P_{POC} fluxes at 100 m range from $0.65 - 7.95 \text{ mmol m}^{-2} \text{d}^{-1}$; they are generally higher in summer than winter, and

375 highest at station P4, consistent with previous studies at Line P (Charette et al., 1999; Wong et
376 al., 1999; Timothy et al., 2013).

377 The ratio of P_{POC} flux to NPP, referred to as the *ThE*-ratio, is an estimate of efficiency of
378 the biological pump (Buesseler, 1998). *ThE*-ratios determined using P_{POC} fluxes at the base of
379 the photic zone (Table 3, Fig. 10) are similar to those reported by Charette et al. (1999), and are
380 also in line with an annual average e-ratio determined using average sediment trap POC fluxes
381 (Wong et al., 1999) and annual average NPP (Harrison, 2002) (Fig. 10).

382

383 3.8 Sediment trap ^{234}Th and POC fluxes

384 The particle fluxes of both ^{234}Th and POC fluxes determined by the PITS traps (F_{Th} and
385 F_{POC} respectively) generally decrease with depth (Table 5). F_{Th} was higher in June 2012 than in
386 June 2011, though there was no clear difference between the two cruises for F_{POC} . A comparison
387 of the F_{Th} with the P_{Th} from corresponding stations and depths indicates that the F_{Th} is
388 consistently higher than the P_{Th} , though usually not by more than a factor of two. F_{POC} is also
389 consistently higher than P_{POC} , though again not by more than a factor of two (Fig. 11a). The
390 POC/ ^{234}Th ratios of particles caught in sediment traps (Table 9) tend to be slightly higher
391 (generally within a factor of 2) than the ratio of particles sampled by pumps at the corresponding
392 station and depth.

393

394 3.9 ^{234}Th -derived and sediment trap pigment fluxes

395 Sinking fluxes of Chl *a* (P_{Chla}) and indicator pigments ($P_{Pigment}$) were calculated from P_{Th}
396 and the Pigment/ ^{234}Th ratio measured on >53- μm particles. Chl *a* and indicator pigment fluxes
397 (Table 4, Fig. 12a-c) are generally highest at station P4 and decrease moving offshore. The
398 highest indicator pigment fluxes were typically observed for microplankton pigments (FUCO
399 and PER) whereas the lowest were observed for the picoplankton pigment ZEA (Table 4, Fig.
400 12a-c). It is important to note that the differences between fluxes of different pigments at a given
401 station are determined by the pigment ratio on the >53- μm particles and are independent of P_{Th} .

402 Sediment trap pigment fluxes ($F_{Pigment}$) were typically lower than $P_{Pigment}$ (Table 4, Fig.
403 11b). The maximum sediment trap fluxes of Chl *a* and most indicator pigments were determined
404 at 50 m in June 2011 and at 30 m in June 2012 (Table 4). For both deployments the deepest
405 fluxes were generally the lowest, presumably due to the progressive degradation of sinking

Brendan Mackinson 4/2/2015 9:28 PM
Deleted: 2

Brendan Mackinson 4/2/2015 9:26 PM
Deleted: 4

Brendan Mackinson 4/2/2015 9:27 PM
Deleted: 3

Brendan Mackinson 4/2/2015 9:27 PM
Deleted: 3

Brendan Mackinson 4/2/2015 9:27 PM
Deleted: 3

Brendan Mackinson 4/2/2015 9:27 PM
Deleted: 3

412 phytoplankton and resulting loss of pigments. Chl *a* and indicator pigment fluxes were generally
413 higher in June 2011 than in June 2012, which is the opposite of the trend observed for F_{Th} .

414 Pigment PFs determined for material captured by the PITS traps do not vary greatly with
415 depth, suggesting that the quality of material sinking to depth is similar to that in the surface
416 water, despite the general decrease of material (Figs. 6 and 8). Microplankton PFs are higher for
417 trap samples than for bottle samples but not as high as for pump samples, while nPFs and pPFs
418 are higher for trap samples than for pump samples but lower than for bottle samples.

419

420 4 Discussion

421 The results presented in this study build on previous investigations of export production
422 in the northeast Pacific by providing estimates of the relative contributions of different
423 phytoplankton size-classes to particle export. A comparison of indicator pigment standing stocks
424 determined from small-volume samples and $P_{Pigment}$ fluxes suggests that while nanoplankton
425 represented the bulk of phytoplankton biomass ($68 \pm 24\%$ of pigment standing stock, averaged for
426 all stations and cruises), microplankton dominated the flux of pigmented material ($69 \pm 19\%$ on
427 average) (Table 4, Fig. 12). Sediment trap pigment fluxes indicate a lower, but still substantial,
428 relative contribution of microplankton to export, with microplankton pigments making up 47%
429 and 33% of the total sediment trap indicator pigment flux in June 2011 and June 2012
430 respectively, as compared to 81% and 85% of total $P_{Pigment}$ fluxes. Though nano- and
431 picoplankton did not form the majority of the algal aggregate flux, their $29 \pm 19\%$ contribution is
432 significant and similar to contributions reported by Lomas and Moran (2011) for cyanobacteria
433 and nano-eukaryotes in the Sargasso Sea.

434 Indicator pigment loss rates determined from both $P_{Pigment}$ fluxes and sediment trap
435 pigment fluxes imply that microplankton are exported more efficiently than nano- or
436 picoplankton (Table 4, Fig. 12d-f). Loss rates of pigments, estimated as the ratio of $P_{Pigment}$
437 fluxes to pigment standing stock, averaged (for all cruises) $8 \pm 12\%$ for microplankton pigments,
438 $1 \pm 2\%$ for nanoplankton pigments and $0.6 \pm 1\%$ for picoplankton pigments. These results suggest
439 that export of large cells by direct sinking of algal aggregates is more efficient than the export of
440 small cells by the same pathway. Sediment trap loss rates for microplankton were also higher
441 than those for nano- and picoplankton, further indicating preferential export of microplankton.
442 Even though differences between bottle and pump samples may exaggerate the extent to which

Brendan Mackinson 4/2/2015 9:27 PM

Deleted: 3

Brendan Mackinson 4/2/2015 9:27 PM

Deleted: 3

445 large cells dominate export, sediment trap loss rates support and confirm the preferential export
446 of large cells by algal aggregation.

447 In contrast to the trends observed for pigment fluxes and loss rates, the low variability of
448 pump indicator pigment PFs with depth (Figs. 6-8) does not appear to indicate preferential export
449 of microplankton. Furthermore, the presence of nano- and picoplankton pigments in the >53- μ m
450 size-fraction and in samples below the mixed layer suggests that nano- and picoplankton are
451 incorporated into aggregates and that some of these aggregates are exported from the surface
452 ocean. If large cells were being preferentially exported, microplankton pigments would be
453 expected to make up a larger percentage of total pigments in samples below the mixed layer than
454 in samples from the mixed layer, but this is not observed in the results of this study. It is
455 possible that some of this discrepancy can be attributed to differences between bottle and pump
456 samples. Because cells <1- μ m in size can pass through the 1- μ m Nitex screens used in the
457 pumps, the sum of the pump size-fractions does not accurately reflect the community
458 composition in the euphotic zone, and may miss a change in indicator pigment PFs with depth.
459 In addition, the under-sampling of large cells by Niskin bottles may lead to an underestimate of
460 microplankton standing stocks, and thus and overestimate of microplankton loss rates.

461 These pigment fluxes are likely lower estimates of the total contribution of each
462 phytoplankton group to particle export. The use of indicator pigments as tracers of
463 phytoplankton export only accounts for the direct sinking of healthy, ungrazed cells, because
464 grazing degrades the indicator pigments to an analytically undetectable form (Head and Harris,
465 1992; Strom et al., 1998; Thibault et al., 1999). Indirect export (via grazing) is thought to be an
466 important pathway for picoplankton export in the HNLC Equatorial Pacific (Richardson et al.,
467 2004; Stukel and Landry, 2010). Given that grazing has been shown to control the biomass of
468 small phytoplankton in the northeast Pacific (Landry et al., 1993; Harrison et al., 1999; Rivkin et
469 al., 1999), indirect export may also be a significant pathway for small cell export in this region.
470 Because this pathway is not accounted for by the methodology employed in this study, the results
471 presented here may underestimate the export of small phytoplankton, which may be less likely to
472 sink directly. It is also possible that grazing contributes further to enhanced export of large
473 phytoplankton as suggested by traditional models of the biological pump (e.g., Michaels and
474 Silver 1988).

475 Although grazing and fecal pellet export were not directly measured in this study, a
476 comparison of sediment trap and pump measurements of Chl *a*, indicator pigments, and POC,
477 suggests that zooplankton fecal pellets may be an important component of POC export at OSP, at
478 least in spring (Fig. 11). While F_{POC} fluxes are higher than the corresponding P_{POC} fluxes,
479 $F_{Pigment}$ fluxes are lower than $P_{Pigment}$ fluxes, indicating that the material captured by the sediment
480 traps is enriched in carbon and depleted in Chl *a* and indicator pigments relative to that sampled
481 by the pumps. Because the trap brine was not poisoned, zooplankton grazing and cell
482 degradation in the trap tube may also have contributed to some loss of pigments over the ~3 day
483 deployment of the PITS traps. However, the collection of carbon-rich and pigment-depleted
484 fecal pellets by the traps but not by the pumps, which do not quantitatively sample fecal pellets
485 (Lomas and Moran, 2011), could also explain these observations. This latter explanation is
486 consistent with the results presented in Thibault et al. (1999), which indicate that fecal pellet
487 export is 3 to 6 times greater than algal aggregate export at Line P.

488

489 5 Conclusions

490 New estimates of phytoplankton indicator pigment loss rates calculated from both ^{234}Th -
491 derived and sediment trap pigment fluxes suggest that large cells are preferentially exported at
492 Line P. Specifically, microplankton pigments on average made up $69 \pm 19\%$ of the total pigment
493 flux, but only $32 \pm 24\%$ of pigment standing stock (determined from small-volume samples),
494 whereas nano- and picoplankton pigments on average formed $31 \pm 19\%$ of pigment flux in spite of
495 representing $68 \pm 24\%$ of the standing stock. These results are consistent with traditional food
496 web models (Michaels and Silver, 1988; Legendre and Le Fèvre, 1995) that suggest nano- and
497 picoplankton are underrepresented in particle flux relative to their contribution to phytoplankton
498 biomass; they also lend support to the conclusions of Choi et al. (2014). However, the methods
499 employed in this study do not quantitatively account for export via zooplankton fecal pellets,
500 which could be significant for small phytoplankton as they are controlled by grazing in this
501 region (Landry et al., 1993; Harrison et al., 1999; Rivkin et al., 1999; Thibault et al., 1999).
502 Furthermore, the determination of pigment loss rates also required a comparison between small-
503 and large-volume samples, and the inherent differences of these sampling techniques likely led to
504 an overestimation of the microplankton contribution to algal aggregate export. Therefore, it is

possible that all sizes-classes of phytoplankton contribute to POC export in approximate proportion to their contribution to NPP as predicted by Richardson and Jackson (2007).

This study, conducted in a subarctic HNLC region, contributes to the ongoing discussion of small cell export that has largely focused on tropical and subtropical regions (Richardson et al., 2004; Richardson et al., 2006; Richardson and Jackson, 2007; Stukel and Landry, 2010; Lomas and Moran, 2011). In particular, these results suggest that nano- and picoplankton may contribute significantly to POC export in this subarctic HNLC region, even if they are not as efficiently exported as larger microplankton. If large phytoplankton drive more efficient POC export in the northeast Pacific as suggested by this study, it could have important implications for understanding the biological pump. It has been proposed that decreasing winter mixed layer depths (Freeland et al., 1997; Freeland, 2013) and variations of macronutrient concentrations linked to shifts in climate regime (Pena and Varela, 2007) in the northeast Pacific could lead to shifts in the phytoplankton community composition. This study suggests that such changes in phytoplankton community composition could significantly affect the efficiency of the biological pump, and in turn, the cycling of carbon. While the results indicate that shifts in community composition favoring larger phytoplankton could lead to more efficient particle export, they do not indicate that shifts favoring smaller phytoplankton would lead to a shutdown of POC export as suggested by some previous studies (e.g., Michaels and Silver, 1988), but merely that the export of POC could be less efficient.

Acknowledgements

We thank the captain and crew of the CCGS *John P. Tully*, Marie Robert and the Line P Program collaborators, Doug Bell for at-sea sampling and laboratory assistance, and Matthew Baumann for his laboratory assistance. This research was supported by the National Science Foundation grants OCE 0926311 to SBM, OCE 0927559 to MWL, and OCE 0926348 to GMS.

536

537

538

539

540 **References**

- 541 Amacher, J., Neuer, S., Anderson, I. and Massana, R.: Molecular approach to determine
542 contributions of the protist community to particle flux, *Deep-Sea Res. Part Oceanogr. Res. Pap.*,
543 56(12), 2206–2215, doi:10.1016/j.dsr.2009.08.007, 2009.
- 544 Baumann, M. S., Moran, S. B., Lomas, M. W., Kelly, R. P. and Bell, D. W.: Seasonal decoupling
545 of particulate organic carbon export and net primary production in relation to sea-ice at the shelf
546 break of the eastern Bering Sea: Implications for off-shelf carbon export, *J. Geophys. Res.*
547 *Oceans*, 118(10), 5504–5522, doi:10.1002/jgrc.20366, 2013.
- 548 Benitez-Nelson, C. R., Buesseler, K. O., Van der Loeff, M. R., Andrews, J., Ball, L., Crossin, G.
549 and Charette, M. A.: Testing a new small-volume technique for determining ²³⁴Th in seawater,
550 *J. Radioanal. Nucl. Chem.*, 248(3), 795–799, 2001.
- 551 Bograd, S. J., Thomson, R. E., Rabinovich, A. B. and LeBlond, P. H.: Near-surface circulation of
552 the northeast Pacific Ocean derived from WOCE-SVP satellite-tracked drifters, *Deep Sea Res.*
553 *Part II Top. Stud. Oceanogr.*, 46(11–12), 2371 – 2403, doi:http://dx.doi.org/10.1016/S0967-
554 0645(99)00068-5, 1999.
- 555 Boyd, P. and Harrison, P. J.: Phytoplankton dynamics in the {NE} subarctic Pacific, *Deep Sea*
556 *Res. Part II Top. Stud. Oceanogr.*, 46(11–12), 2405 – 2432, doi:http://dx.doi.org/10.1016/S0967-
557 0645(99)00069-7, 1999.
- 558 Boyd, P. W. and Newton, P. P.: Does planktonic community structure determine downward
559 particulate organic carbon flux in different oceanic provinces?, *Deep Sea Res. Part Oceanogr.*
560 *Res. Pap.*, 46(1), 63 – 91, doi:http://dx.doi.org/10.1016/S0967-0637(98)00066-1, 1999.
- 561 Brew, H. S., Moran, S. B., Lomas, M. W. and Burd, A. B.: Plankton community composition,
562 organic carbon and thorium-234 particle size distributions, and particle export in the Sargasso
563 Sea, *J. Mar. Res.*, 67(6), 845–868, doi:10.1357/002224009792006124, 2009.
- 564 Buesseler, K. O.: The decoupling of production and particulate export in the surface ocean, *Glob.*
565 *Biogeochem. Cycles*, 12(2), 297–310, doi:10.1029/97GB03366, 1998.
- 566 Buesseler, K. O., Benitez-Nelson, C., Rutgers van der Loeff, M., Andrews, J., Ball, L., Crossin,
567 G. and Charette, M. A.: An intercomparison of small-and large-volume techniques for thorium-
568 ²³⁴Th in seawater, *Mar. Chem.*, 74(1), 15–28, 2001.
- 569 Burd, A. B., Jackson, G. A. and Moran, S. B.: The role of the particle size spectrum in estimating
570 POC fluxes from disequilibrium, *Deep Sea Res. Part Oceanogr. Res. Pap.*, 54(6), 897–918, 2007.

571 Charette, M. A., Moran, S. B. and Bishop, J. K. B.: ²³⁴Th as a tracer of particulate organic
572 carbon export in the subarctic northeast Pacific Ocean, *Deep Sea Res. Part II Top. Stud.*
573 *Oceanogr.*, 46(11–12), 2833 – 2861, doi:http://dx.doi.org/10.1016/S0967-0645(99)00085-5,
574 1999.

575 Chen, J. H., Lawrence Edwards, R. and Wasserburg, G. J.: ²³⁸U, ²³⁴U and ²³²Th in seawater,
576 *Earth Planet. Sci. Lett.*, 80(3), 241–251, 1986.

577 Choi, H. Y., Stewart, G. M., Lomas, M. W., Kelly, R. P. and Moran, S. B.: Linking the
578 distribution of ²¹⁰Po and ²¹⁰Pb with plankton community along
579 Line P, Northeast Subarctic Pacific, *J. Environ. Radioact.*, 2014.

580 Coale, K. H. and Bruland, K. W.: ²³⁴Th: ²³⁸U disequilibria within the California Current,
581 *Limnol Ocean.*, 30(1), 22–33, 1985.

582 Emerson, S.: Annual net community production and the biological carbon flux in the ocean,
583 *Glob. Biogeochem. Cycles*, 2014.

584 Freeland, H., Denman, K., Wong, C. S., Whitney, F. and Jacques, R.: Evidence of change in the
585 winter mixed layer in the Northeast Pacific Ocean, *Deep Sea Res. Part Oceanogr. Res. Pap.*,
586 44(12), 2117 – 2129, doi:http://dx.doi.org/10.1016/S0967-0637(97)00083-6, 1997.

587 Freeland, H. J.: Evidence of Change in the Winter Mixed Layer in the Northeast Pacific Ocean:
588 A Problem Revisited, *Atmosphere-Ocean*, 51(1), 126–133, 2013.

589 Gardner, W. D.: Incomplete extraction of rapidly settling particles from water samplers, *Limnol*
590 *Ocean.*, 22(4), 764–768, 1977.

591 Gundersen, K., Orcutt, K. M., Purdie, D. A., Michaels, A. F. and Knap, A. H.: Particulate
592 organic carbon mass distribution at the Bermuda Atlantic Time-series Study (BATS) site, *Deep*
593 *Sea Res. Part II Top. Stud. Oceanogr.*, 48(8), 1697–1718, 2001.

594 Harrison, P. J.: SERIES (subarctic ecosystem response to iron enrichment study): A Canadian–
595 Japanese contribution to our understanding of the iron–ocean–climate connection, *Deep Sea Res.*
596 *Part II Top. Stud. Oceanogr.*, 53(20), 2006.

597 Harrison, P. J., Boyda, P. W., Varela, D. E., Takeda, S., Shiomoto, A. and Odate, T.:
598 Comparison of factors controlling phytoplankton productivity in the {NE} and {NW} subarctic
599 Pacific gyres, *Prog. Oceanogr.*, 43(2–4), 205 – 234, doi:http://dx.doi.org/10.1016/S0079-
600 6611(99)00015-4, 1999.

601 Head, E. J. H. and Harris, L. R.: Chlorophyll and carotenoid transformation and destruction by
602 *Calanus* spp. grazing on diatoms, *Mar. Ecol.-Prog. Ser.*, 86, 229–229, 1992.

603 Hooker, S. B., Van Heukelem, L., Thomas, C. S., Claustre, H., Ras, J., Barlow, R., Sessions, H.,
604 Schlüter, L., Perl, J. and Trees, C.: Second SeaWiFS HPLC Analysis Round-robin Experiment
605 (SeaHARRE-2), National Aeronautics and Space Administration, Goddard Space Flight Center.,
606 2005.

607 Irwin, A. J., Finkel, Z. V., Schofield, O. M. E. and Falkowski, P. G.: Scaling-up from nutrient
 608 physiology to the size-structure of phytoplankton communities, *J. Plankton Res.*, 28(5), 459–471,
 609 doi:10.1093/plankt/fbi148, 2006.

610 Knap, A. H., Michaels, A. F., Steinberg, D. K., Bahr, F., Bates, N. R., Bell, S., Countway, P.,
 611 Close, A. R., Doyle, A. P. and Dow, R. L.: BATS Methods manual, version 4,, 1997.

612 Landry, M. R., Monger, B. C. and Selph, K. E.: Time-dependency of microzooplankton grazing
 613 and phytoplankton growth in the subarctic Pacific, *Prog. Oceanogr.*, 32(1–4), 205 – 222,
 614 doi:http://dx.doi.org/10.1016/0079-6611(93)90014-5, 1993.

615 Legendre, L. and Le Fèvre, J.: Microbial food webs and the export of biogenic carbon in oceans,
 616 *Aquat. Microb. Ecol.*, 9(1), 69–77, 1995.

617 Liu, Z., Cochran, J. K., Lee, C., Gasser, B., Miquel, J. C. and Wakeham, S. G.: Further
 618 investigations on why {POC} concentrations differ in samples collected by Niskin bottle and in
 619 situ pump, *Deep Sea Res. Part II Top. Stud. Oceanogr.*, 56(18), 1558 – 1567,
 620 doi:http://dx.doi.org/10.1016/j.dsr2.2008.12.019, 2009.

621 Liu, Z., Stewart, G., Kirk Cochran, J., Lee, C., Armstrong, R. A., Hirschberg, D. J., Gasser, B.
 622 and Miquel, J.-C.: Why do POC concentrations measured using Niskin bottle collections
 623 sometimes differ from those using in-situ pumps?, *Deep Sea Res. Part Oceanogr. Res. Pap.*,
 624 52(7), 1324–1344, doi:10.1016/j.dsr.2005.02.005, 2005.

625 Van der Loeff, M. R., Sarin, M. M., Baskaran, M., Benitez-Nelson, C., Buesseler, K. O.,
 626 Charette, M., Dai, M., Gustafsson, Ö., Masque, P. and Morris, P. J.: A review of present
 627 techniques and methodological advances in analyzing²³⁴Th in aquatic systems,
 628 *Mar. Chem.*, 100(3), 190–212, 2006.

629 Lomas, M. W. and Moran, S. B.: Evidence for aggregation and export of cyanobacteria and
 630 nano-eukaryotes from the Sargasso Sea euphotic zone, *Biogeosciences*, 8(1), 203–216,
 631 doi:10.5194/bg-8-203-2011, 2011.

632 Lomas, M. W., Moran, S. B., Casey, J. R., Bell, D. W., Tiahlo, M., Whitefield, J., Kelly, R. P.,
 633 Mathis, J. T. and Cokelet, E. D.: Spatial and seasonal variability of primary production on the
 634 Eastern Bering Sea shelf, *Deep Sea Res. Part II Top. Stud. Oceanogr.*, 65–70(0), 126 – 140,
 635 doi:http://dx.doi.org/10.1016/j.dsr2.2012.02.010, 2012.

636 Marchetti, A., Sherry, N. D., Kiyosawa, H., Tsuda, A. and Harrison, P. J.: Phytoplankton
 637 processes during a mesoscale iron enrichment in the NE subarctic Pacific: Part I—biomass and
 638 assemblage, *Deep Sea Res. Part II Top. Stud. Oceanogr.*, 53(20), 2095–2113, 2006.

639 McNally, G. J.: Satellite - tracked drift buoy observations of the near - surface flow in the
 640 eastern mid - latitude North Pacific, *J. Geophys. Res. Oceans* 1978–2012, 86(C9), 8022–8030,
 641 1981.

642 Michaels, A. F. and Silver, M. W.: Primary production, sinking fluxes and the microbial food
 643 web, *Deep Sea Res. Part Oceanogr. Res. Pap.*, 35(4), 473 – 490,
 644 doi:[http://dx.doi.org/10.1016/0198-0149\(88\)90126-4](http://dx.doi.org/10.1016/0198-0149(88)90126-4), 1988.

645 Moran, S. B., Charette, M. A., Pike, S. M. and Wicklund, C. A.: Differences in seawater
 646 particulate organic carbon concentration in samples collected using small-and large-volume
 647 methods: the importance of DOC adsorption to the filter blank, *Mar. Chem.*, 67(1), 33–42, 1999.

648 Moran, S. B., Weinstein, S. E., Edmonds, H. N., Smith, J. N., Kelly, R. P., Pilson, M. E. Q. and
 649 Harrison, W. G.: Does $^{234}\text{Th}/^{238}\text{U}$ disequilibrium provide an accurate record of the export flux
 650 of particulate organic carbon from the upper ocean?, *Limnol. Oceanogr.*, 48(3), 1018–1029,
 651 2003.

652 Morán, X. A. G., López-Urrutia, Á., Calvo - Díaz, A. and Li, W. K.: Increasing importance of
 653 small phytoplankton in a warmer ocean, *Glob. Change Biol.*, 16(3), 1137–1144, 2010.

654 Muggli, D. L., Lecourt, M. and Harrison, P. J.: Effects of iron and nitrogen source on the sinking
 655 rate, physiology and metal composition of an oceanic diatom from the subarctic Pacific,
 656 *Oceanogr. Lit. Rev.*, 43(11), 1996.

657 Pena, M. A. and Varela, D. E.: Seasonal and interannual variability in phytoplankton and nutrient
 658 dynamics along Line P in the NE subarctic Pacific, *Prog. Oceanogr.*, 75(2), 200–222, 2007.

659 Polovina, J. J., Howell, E. A. and Abecassis, M.: Ocean's least productive waters are expanding,
 660 *Geophys. Res. Lett.*, 35(3), 2008.

661 Richardson, T. L. and Jackson, G. A.: Small phytoplankton and carbon export from the surface
 662 ocean, *Science*, 315(5813), 838–840, 2007.

663 Richardson, T. L., Jackson, G. A., Ducklow, H. W. and Roman, M. R.: Carbon fluxes through
 664 food webs of the eastern equatorial Pacific: an inverse approach, *Deep Sea Res. Part Oceanogr.*
 665 *Res. Pap.*, 51(9), 1245–1274, doi:[10.1016/j.dsr.2004.05.005](https://doi.org/10.1016/j.dsr.2004.05.005), 2004.

666 Richardson, T. L., Jackson, G. A., Ducklow, H. W. and Roman, M. R.: Spatial and seasonal
 667 patterns of carbon cycling through planktonic food webs of the Arabian Sea determined by
 668 inverse analysis, *US JGOFS Synth. Model. Proj. Phase III US JGOFS Synth. Model. Proj. Phase*
 669 *III*, 53(5–7), 555–575, doi:[10.1016/j.dsr2.2006.01.015](https://doi.org/10.1016/j.dsr2.2006.01.015), 2006.

670 Rivkin, R. B., Putland, J. N., Robin Anderson, M. and Deibel, D.: Microzooplankton bacterivory
 671 and herbivory in the NE subarctic Pacific, *Deep Sea Res. Part II Top. Stud. Oceanogr.*, 46(11),
 672 2579–2618, 1999.

673 Speicher, E. A., Moran, S. B., Burd, A. B., Delfanti, R., Kaberi, H., Kelly, R. P., Papucci, C.,
 674 Smith, J. N., Stavrakakis, S. and Torricelli, L.: Particulate organic carbon export fluxes and size-
 675 fractionated POC/²³⁴Th ratios in the Ligurian, Tyrrhenian and Aegean Seas,
 676 *Deep Sea Res. Part Oceanogr. Res. Pap.*, 53(11), 1810–1830, 2006.

677 Strom, S., Morello, T. and Bright, K.: Protozoan size influences algal pigment degradation
678 during grazing, *Mar. Ecol. Prog. Ser.* Halstenbek, 164, 189–197, doi:10.3354/meps164189,
679 1998.

680 Stukel, M. R., Décima, M., Selph, K. E., Taniguchi, D. A. and Landry, M. R.: The role of
681 *Synechococcus* in vertical flux in the Costa Rica upwelling dome, *Prog. Oceanogr.*, 112, 49–59,
682 2013.

683 Stukel, M. R. and Landry, M. R.: Contribution of picophytoplankton to carbon export in the
684 equatorial Pacific: A reassessment of food web flux inferences from inverse models, *Limnol.*
685 *Oceanogr.*, 55(6), 2669–2685, 2010.

686 Thibault, D., Roy, S., Wong, C. S. and Bishop, J. K.: The downward flux of biogenic material in
687 the NE subarctic Pacific: importance of algal sinking and mesozooplankton herbivory, *Deep Sea*
688 *Res. Part II Top. Stud. Oceanogr.*, 46(11), 2669–2697, 1999.

689 Timothy, D. A., Wong, C. S., Barwell-Clarke, J. E., Page, J. S., White, L. A. and Macdonald, R.
690 W.: Climatology of sediment flux and composition in the subarctic Northeast Pacific Ocean with
691 biogeochemical implications, *Prog. Oceanogr.*, 116, 95–129, 2013.

692 Wong, C. S., Whitney, F. A., Crawford, D. W., Iseki, K., Matear, R. J., Johnson, W. K., Page, J.
693 S. and Timothy, D.: Seasonal and interannual variability in particle fluxes of carbon, nitrogen
694 and silicon from time series of sediment traps at Ocean Station P, 1982–1993: Relationship to
695 changes in subarctic primary productivity, *Deep Sea Res. Part II Top. Stud. Oceanogr.*, 46(11),
696 2735–2760, 1999.

697
698
699
700
701
702
703
704
705
706
707
708
709
710

Brendan Mackinson 4/7/2015 12:57 AM
Deleted: - ... (1)

Table 1: Summary of abbreviations used

<u>Term</u>	<u>Abbreviation</u>	<u>Unit</u>
<u>net primary production</u>	<u>NPP</u>	<u>mmol m⁻² d⁻¹</u>
<u>suspended particulate organic carbon</u>	<u>POC</u>	<u>umol L⁻¹</u>
<u>²³⁴Th activity</u>	<u>²³⁴Th</u>	<u>dpm L⁻¹</u>
<u>²³⁸U activity</u>	<u>²³⁸U</u>	<u>dpm L⁻¹</u>
<u>chlorophyll <i>a</i> concentration</u>	<u>Chl <i>a</i></u>	<u>ng L⁻¹</u>
<u>fucoxanthin concentration</u>	<u>FUCO</u>	<u>ng L⁻¹</u>
<u>peridinin concentration</u>	<u>PER</u>	<u>ng L⁻¹</u>
<u>19'-hexanoyloxyfucoxanthin concentration</u>	<u>HEX</u>	<u>ng L⁻¹</u>
<u>19'-butanoyloxyfucoxanthin concentration</u>	<u>BUT</u>	<u>ng L⁻¹</u>
<u>alloxanthin concentration</u>	<u>ALLO</u>	<u>ng L⁻¹</u>
<u>total chlorophyll <i>b</i> concentration</u>	<u>TChl <i>b</i></u>	<u>ng L⁻¹</u>
<u>zeaxanthin concentration</u>	<u>ZEA</u>	<u>ng L⁻¹</u>
<u>microplankton proportion factor</u>	<u>mPF</u>	-
<u>nanoplankton proportion factor</u>	<u>nPF</u>	-
<u>picoplankton proportion factor</u>	<u>pPF</u>	-
<u>²³⁴Th flux</u>	<u>P_{Th}</u>	<u>dpm m⁻² d⁻¹</u>
<u>²³⁴Th-derived POC flux</u>	<u>P_{POC}</u>	<u>mmol m⁻² d⁻¹</u>
<u>²³⁴Th-derived e-ratio (P_{POC}/NPP)</u>	<u>ThE-ratio</u>	-
<u>sediment trap ²³⁴Th flux</u>	<u>F_{Th}</u>	<u>dpm m⁻² d⁻¹</u>
<u>sediment trap POC flux</u>	<u>F_{POC}</u>	<u>mmol m⁻² d⁻¹</u>

<u>^{234}Th-derived pigment flux</u>	<u>P_{Pigment}</u>	<u>$\text{mg m}^{-2} \text{d}^{-1}$</u>
<u>sediment trap pigment flux</u>	<u>F_{Pigment}</u>	<u>$\text{mg m}^{-2} \text{d}^{-1}$</u>

Table 2: Cruise dates and sample collection along Line P

Cruise Dates	P4	P12	P16	P20	P26
2010-14 Aug. 2010 (8/19/10 - 8/31/10)	Total Th	Total Th	Total Th	Total Th	Total Th
		WC Pig	WC Pig	WC Pig	
2011-01 Feb. 2011 (2/9/11 - 2/15/11)		Total Th	Total Th	Total Th	Total Th
		WC Pig	WC Pig	WC Pig	
2011-26 June 2011 (6/4/11 - 6/16/11)	Total Th	Total Th	Total Th	Total Th	Total Th
	WC Pig	WC Pig	WC Pig	WC Pig	Part. Th WC Pig Part. Pig Traps
2012-01 Feb. 2012 (2/7/12 - 2/19/12)	Total Th Part. Th WC Pig Part. Pig	Total Th Part. Th WC Pig Part. Pig	Total Th	Total Th	Total Th Part. Th WC Pig Part. Pig
2012-12 June 2012 (5/23/12 - 6/7/12)	Total Th Part. Th WC Pig Part. Pig	Total Th Part. Th WC Pig Part. Pig	Total Th Part. Th WC Pig Part. Pig	Total Th Part. Th Part. Pig	Total Th Part. Th Part. Pig Traps

Brendan Mackinson 4/2/2015 9:26 PM

Deleted: 1

Table 3: Total net primary production (NPP) and >5 μm size-fractionated NPP determined from simulated in situ incubations. ^{234}Th -derived POC flux (P_{POC}) and sediment trap POC flux (F_{POC}) determined at the base of the photic zone and the corresponding ThE -ratios ($P_{\text{POC}}/\text{NPP}$) and trap e -ratios ($F_{\text{POC}}/\text{NPP}$). Stations P26-D and P26-R refer to sediment trap deployment and recover stations respectively.

Cruise	Station	Integration Depth (m)	Total NPP ($\text{mmol m}^{-2} \text{d}^{-1}$)	>5 μm NPP ($\text{mmol m}^{-2} \text{d}^{-1}$)	P_{POC} ($\text{mmol m}^{-2} \text{d}^{-1}$)	F_{POC} ($\text{mmol m}^{-2} \text{d}^{-1}$)	ThE -ratio	Trap e -ratio
Feb. 2011	P20	77	36.64	3.26				
June 2011	P26-D	83	105.14	13.67	2.94	5.91	0.03	0.06
	P26-R	85	78.75	12.98	2.75	5.91	0.03	0.08
Feb. 2012	P4	50	27.91	3.58	7.29		0.26	
	P12	95	34.56	4.58	4.65		0.13	
	P26	75	23.41	5.22	0.31		0.01	
June 2012	P4	103	82.36	39.55	7.95		0.10	
	P12	164	40.24	4.16	2.12		0.05	
	P20	115	57.84	4.10	0.54		0.01	
	P26	60	49.45	9.28	2.96	6.55	0.06	0.13

Brendan Mackinson 4/7/2015 12:58 AM

Deleted: Table 2: Total net primary production (NPP) and >5 μm size-fractionated NPP determined from simulated in situ incubations. ^{234}Th -derived POC flux (P_{POC}) and sediment trap POC flux (Trap_{POC}) determined at the base of the photic zone and the corresponding ThE -ratios ($P_{\text{POC}}/\text{NPP}$) and trap e -ratios ($\text{Trap}_{\text{POC}}/\text{NPP}$).

Brendan Mackinson 4/6/2015 9:59 PM

Deleted: Trap

Brendan Mackinson 4/6/2015 10:00 PM

Formatted Table

Brendan Mackinson 4/7/2015 12:58 AM

Deleted: -

Table 4: Chl *a* and indicator pigment standing stocks determined by integrating small volume pigment concentrations (determined by HPLC) across the photic zone, pigment fluxes (^{234}Th and PITS-derived) measured at the base of the photic zone, and pigment loss rates, or the percent of the surface concentration represented by those fluxes. Pigment standing stocks are in mg m^{-2} and pigment fluxes are in $\text{mg m}^{-2} \text{d}^{-1}$.

Brendan Mackinson 4/2/2015 9:26 PM
Deleted: 3

Cruise	Station	Depth	Chl <i>a</i>	FUCO	PER	HEX	BUT	ALLO	Chl <i>b</i>	ZEA
Aug. 2010 (2010-14)	P12	Surface (1-75 m)	23.918	3.498	0.375	7.705	1.165	0.220	4.038	1.435
	P16	Surface (1-75 m)	14.165	1.288	0.340	6.010	1.018	0.065	2.588	0.165
	P20	Surface (1-75 m)	19.040	3.138	0.398	6.298	1.453	0.065	2.620	0.188
Feb. 2011 (2011-01)	P12	Surface (1-65 m)	30.122	2.848	0.379	5.630	2.431	0.838	7.133	0.922
	P16	Surface (1-95 m)	16.230	1.286	0.202	5.728	1.726	0.161	4.439	1.643
	P20	Surface (1-77 m)	55.053	5.207	0.689	18.064	6.697	1.116	11.435	4.516
June 2011 (2011-26)	P4	Surface (1-72 m)	29.791	2.635	0.127	10.619	2.663	0.720	5.836	5.234
	P12	Surface (1-90 m)	26.115	5.060	0.085	11.988	3.263	0.498	2.665	3.063
	P16	Surface (1-105 m)	22.088	4.044	0.104	11.390	2.195	0.181	2.612	1.569
	P20	Surface (1-70 m)	19.421	4.423	0.197	8.132	1.913	0.166	2.090	1.129
	P26	Surface (1-84 m)	29.376	7.239	0.184	10.532	4.406	0.232	3.723	2.663
		Flux at 100 m	0.765	0.474	0.036	0.059	0.0002	0.016	0.028	0.018
		% Flux	2.605	6.548	$\frac{19.76}{2}$	0.564	0.004	6.686	0.753	0.658
		Trap (150 m)	0.125	0.056	0.027	0.049	0.014	-	0.017	0.015
		% Flux	0.424	0.767	$\frac{14.87}{9}$	0.466	0.311	-	0.461	0.545

Feb. 2012 (2012-01)	P4	Surface (1-38 m)	22.684	3.765	-	4.592	1.434	0.917	3.781	0.280
		Flux at 50 m	3.283	1.863		0.811	0.122			
		% Flux	14.471	49.468	-	17.668	8.537	-	-	-
	P12	Surface (1-38 m)	11.003	1.425	0.116	5.606	1.894	0.017	1.915	0.500
		Flux at 100 m	0.046	0.020	0.000	0.014	0.005	0.000	0.000	0.000
		% Flux	0.415	1.381	0.000	0.254	0.249	0.000	0.000	0.000
	P26	Surface (1-38 m)	12.161	2.092	1.218	2.923	1.615	0.137	0.902	0.228
		Flux at 100 m	0.380	0.251	0.035	0.046	0.038	0.000	0.014	0.045
		% Flux	3.126	11.999	2.898	1.581	2.373	0.000	1.524	19.919
June 2012 (2012-12)	P4	Surface (1-103 m)	21.313	31.420	-	5.192	-	-	-	-
		Flux at 200 m	1.076	0.919	0.047	0.126	-	-	-	0.036
		% Flux	5.047	2.926	-	2.435	-	-	-	-
	P12	Surface (1-164 m)	27.677	5.967	-	22.445	6.552	-	-	-
		Flux at 200 m	0.051	0.047	-	0.075	0.010	-	0.025	-
		% Flux	0.185	0.787	-	0.335	0.156	-	-	-
	P16	Surface (1-66 m)	12.830	8.722	-	17.321	4.238	-	0.942	0.777
		Flux at 100 m	0.312	0.319	0.045	0.044	0.007	-	-	-
		% Flux	2.431	3.662	-	0.252	0.174	-	-	-
	P20	Surface (1-115 m)	18.344	33.038	-	13.892	-	-	13.090	3.538
		Flux at 100 m	0.016	0.016	0.004	-	0.002	-	0.005	0.001
		% Flux	0.088	0.049	-	-	-	-	0.036	0.033
	P26	Surface (1-60 m)	14.024	1.977	-	13.572	2.018	-	4.969	2.768
		Flux at 100 m	0.255	0.304	-	-	0.029	-	0.025	-
		% Flux	1.821	15.359	-	-	1.437	-	0.507	-
		Trap (100 m)	0.055	0.025	0.006	0.041	0.004	-	0.009	0.008
		% Flux	0.393	1.243	-	0.304	0.190	-	0.179	0.288

749

750

751

752

Table 5: ^{234}Th and POC fluxes and POC/ ^{234}Th ratios measured by the PITS traps.

Depth (m)	Days In-situ	^{234}Th flux (dpm m ⁻² d ⁻¹)	POC flux (mmol m ⁻² d ⁻¹)	POC/ ^{234}Th ratio (μmol dpm ⁻¹)
June 2011 P26				
30	3.32	3192 ± 117	15.3 ± 0.4	4.8 ± 0.2
50	3.32	2909 ± 92	10.1 ± 0.3	3.5 ± 0.1
100	3.32	2256 ± 94	5.9 ± 0.2	2.6 ± 0.1
150	3.32	1928 ± 79	5.0 ± 0.2	2.6 ± 0.1
200	3.32	2281 ± 97	8.5 ± 0.3	3.7 ± 0.2
June 2012 P26				
30	2.82	3999 ± 206	14.7 ± 0.4	3.7 ± 0.2
50	2.82	5485 ± 290	13.5 ± 0.5	2.5 ± 0.2
100	2.82	3154 ± 192	6.5 ± 0.2	2.1 ± 0.1
150	2.82	2151 ± 135	5.5 ± 0.2	2.5 ± 0.2
200	2.82	3959 ± 129	5.0 ± 0.2	1.3 ± 0.1

Brendan Mackinson 4/2/2015 9:26 PM

Deleted: 4

773 Figure 1. Map showing the Line P stations sampled in this study.
774

775 Figure 2. Temperature ($^{\circ}\text{C}$), Sigma-t (kg m^{-3}), and $^{234}\text{Th}/^{238}\text{U}$ activity ratio distributions along
776 Line P cruises in August 2010, February 2011, June 2011, February 2012, and June 2012.
777

778 Figure 3. Comparison of small-volume Niskin bottle and large-volume in situ pump
779 measurements of a) POC, b) picoplankton indicator pigments, c) nanoplankton indicator
780 pigments, d) microplankton pigments. Niskin bottle measurements are lower than pump
781 measurements for microplankton pigments, and higher for nanoplankton pigments and POC.
782

783 Figure 4. a) $\text{POC}/^{234}\text{Th}$ ratios on 1 – 10- μm particles and on 10 – 53- μm particles plotted against
784 the $\text{POC}/^{234}\text{Th}$ ratio on >53- μm particles. Fractional distributions of POC and particulate ^{234}Th
785 are plotted for three size-classes of particles. The percentage of total POC associated with each
786 particle size-class is plotted against the percentage of total particulate ^{234}Th for samples collected
787 at stations on Line P during b) June 2011, c) February 2012, and d) June 2012. The correlation
788 coefficient (r^2) and the slope of the linear regression (m) are shown for each cruise.
789

790 Figure 5. Pigment Proportion Factors (PF) for each phytoplankton size-class plotted as a
791 function of sample depth at stations sampled on Line P during the five cruises in the study. All
792 data were collected from Niskin bottles.
793

794 Figure 6. Pigment PF for each phytoplankton size group plotted as a function of sample depth
795 and particle size-class at stations sampled on Line P in June 2011. Size-fractionated data are pump
796 data. Sediment trap PF's are also included.
797

798 Figure 7. Pigment PF for each phytoplankton size group plotted as a function of sample depth
799 and particle size-class at stations sampled on Line P in February 2012. Size-fractionated data are
800 pump data.
801

802 Figure 8. Pigment PF for each phytoplankton size group plotted as a function of sample depth
803 and particle size-class at stations sampled on Line P in June 2012. Size-fractionated data are pump
804 data. Sediment trap PF's are also included where available.

805

806 Figure 9. Depth profiles of a) ^{234}Th fluxes (P_{Th}) determined using the 2-D model, b) $\text{POC}/^{234}\text{Th}$
807 ratios on $>53\ \mu\text{m}$ particles, and c) ^{234}Th -derived POC fluxes (P_{POC}) at stations on Line P during
808 the five cruises in this study.

809

810 Figure 10. Net primary production (NPP) plotted against ^{234}Th -derived POC fluxes (P_{POC}) for
811 stations along Line P in this study. The slopes of the dashed lines represent ThE -ratios. For
812 reference NPP and P_{POC} values determined by Charette et al. (1999) for winter, spring and
813 summer are included, along with annual average NPP and sediment trap POC fluxes (at 200 m)
814 reported in Harrison (2002) and Wong et al. (1999) respectively.

815

816 Figure 11. a) Comparison of sediment trap POC fluxes and ^{234}Th -derived POC fluxes, and b) a
817 comparison of sediment trap Chl *a* and total indicator pigment fluxes and ^{234}Th -derived pigments
818 fluxes at OSP during June 2011 and June 2012.

819

820 Figure 12. a-c) ^{234}Th -derived indicator pigment fluxes determined using the $\text{Pigment}/^{234}\text{Th}$ ratio
821 on $>53\text{-}\mu\text{m}$ particles plotted for micro-, nano-, and picoplankton pigments. d-f) Indicator
822 pigment standing stocks plotted against indicator pigment fluxes for micro-, nano-, and
823 picoplankton pigments. The slopes of the dashed lines indicate pigment loss rates. g-i) The
824 contribution to total pigment standing stock plotted against the contribution to total pigment flux
825 for micro-, nano-, and picoplankton pigments. Data points above the 1:1 line indicate
826 preferential export by direct sinking and points below the 1:1 line indicate disproportionately low
827 export by direct sinking relative to biomass contributions.

828

829

830

831

832

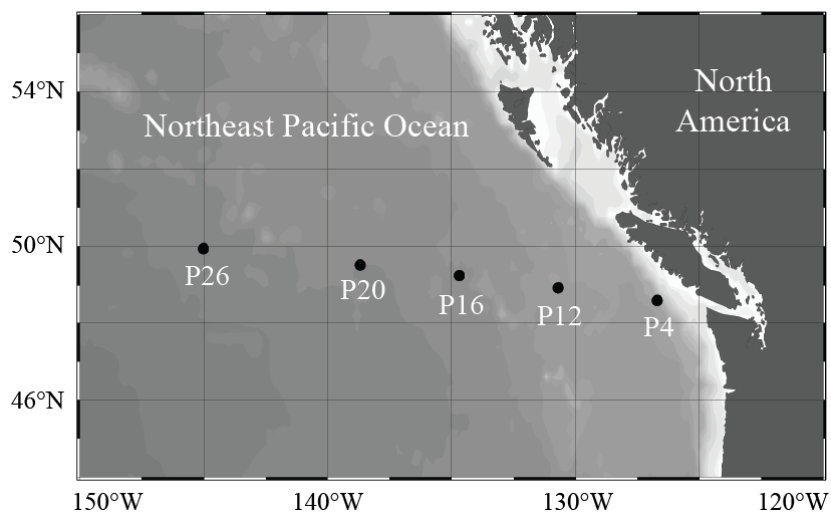


Fig. 1.

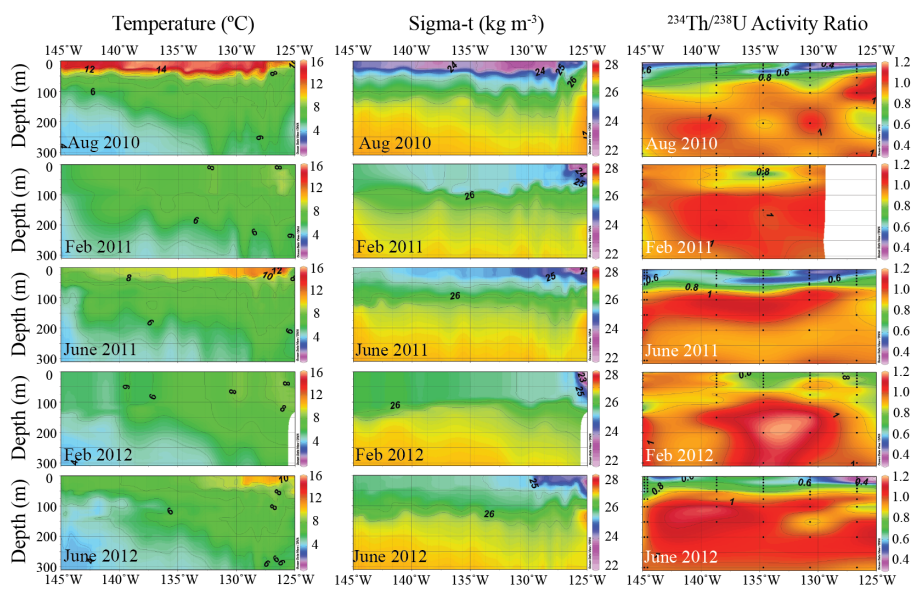


Fig. 2.

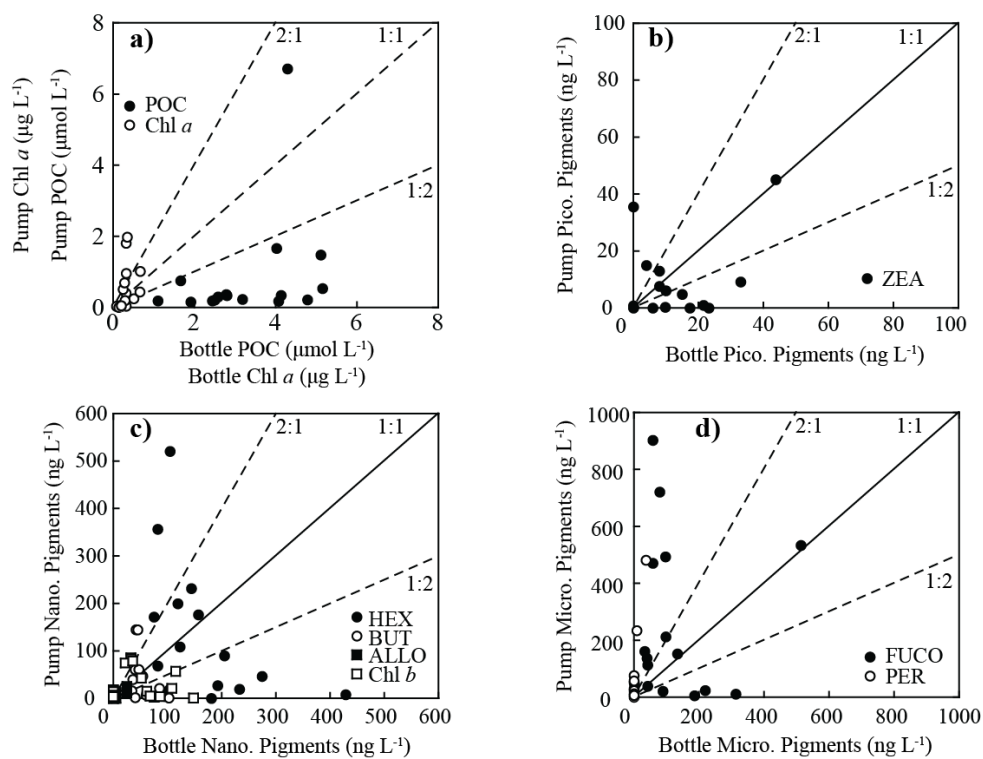


Fig. 3.

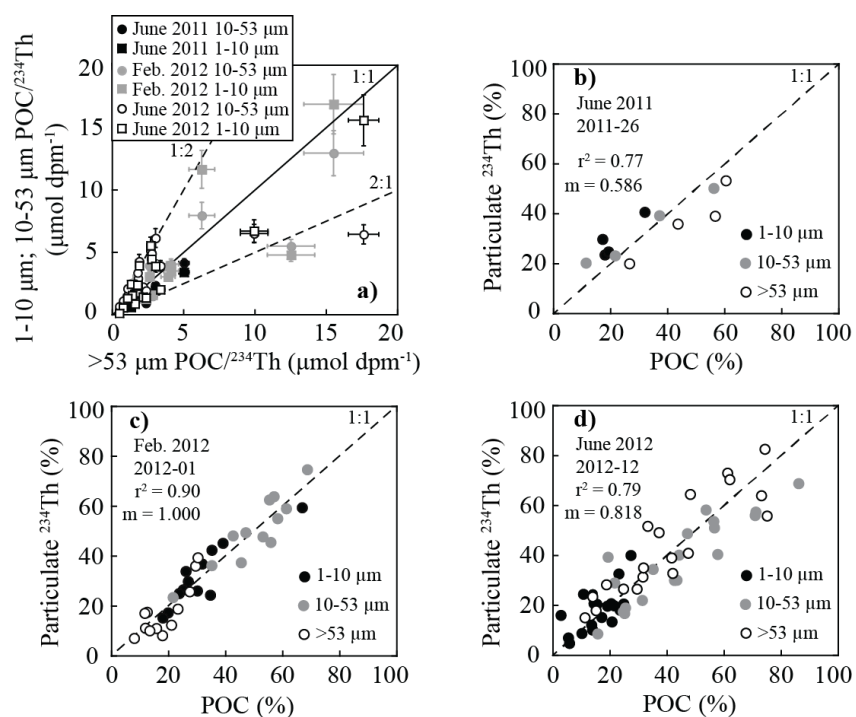


Fig. 4.

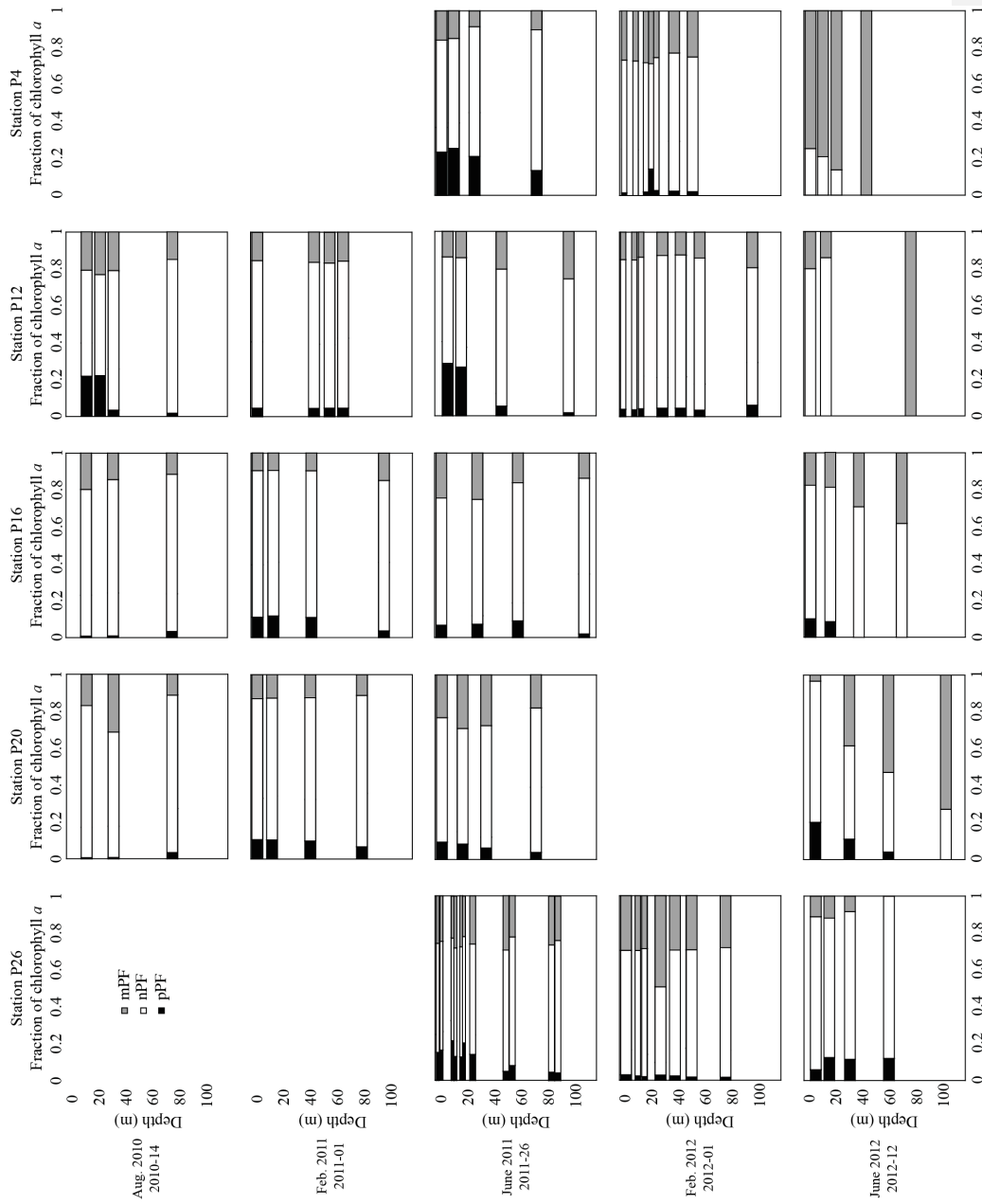
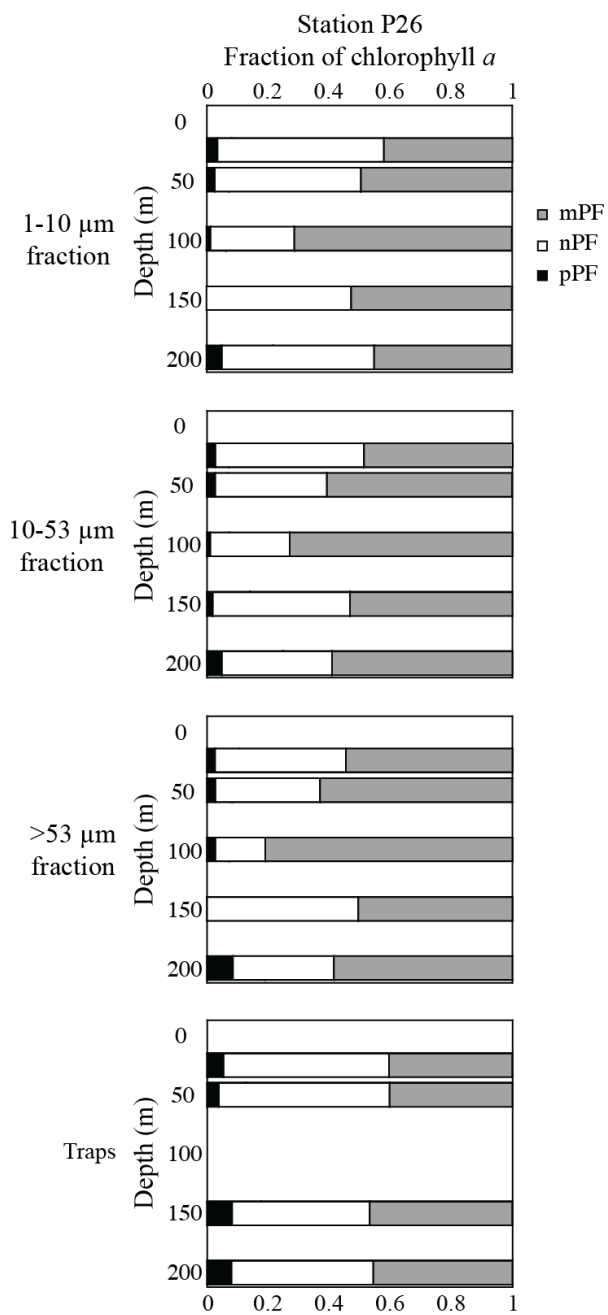


Fig. 5.



886 Fig. 6.
887

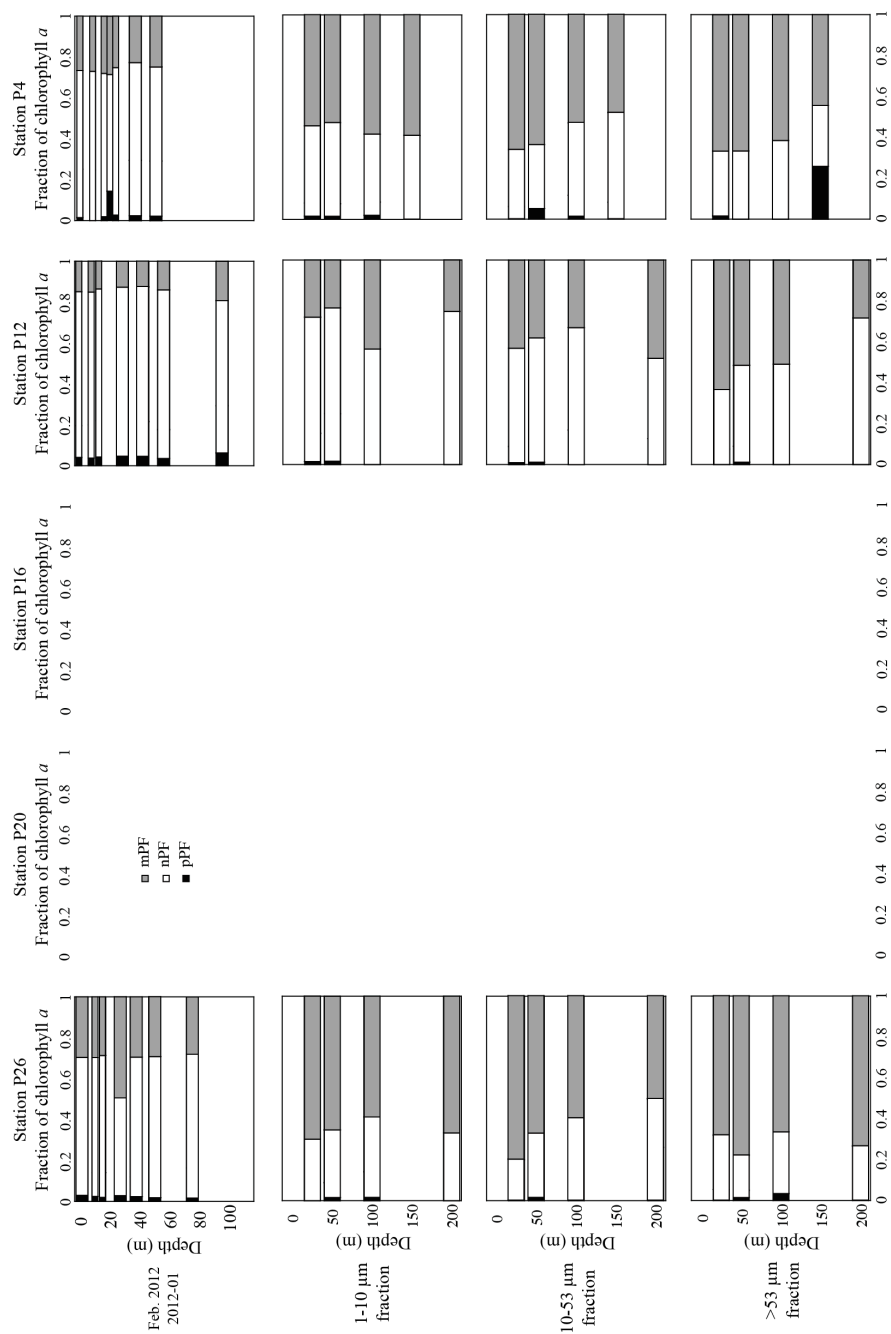


Fig. 7.

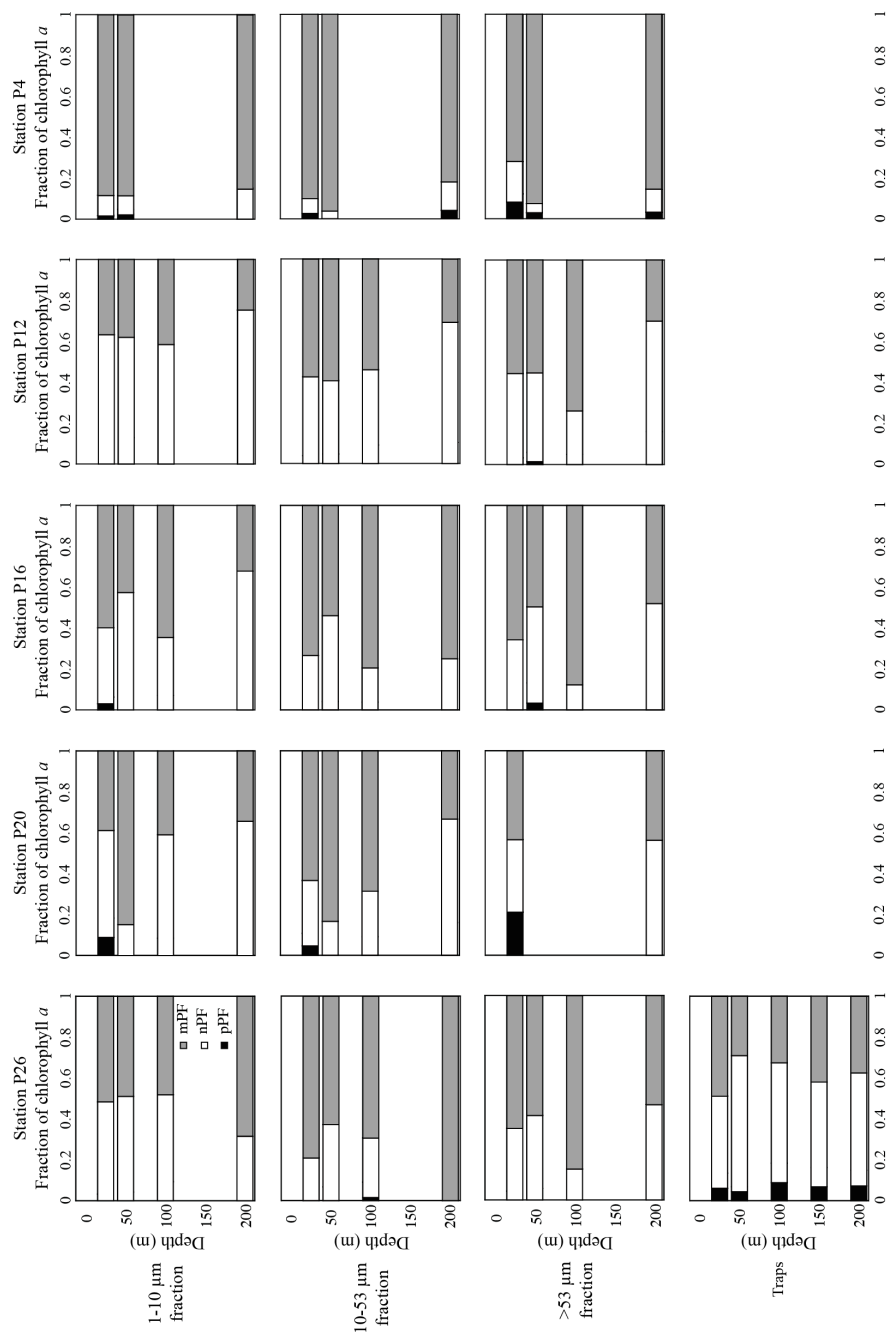


Fig. 8.

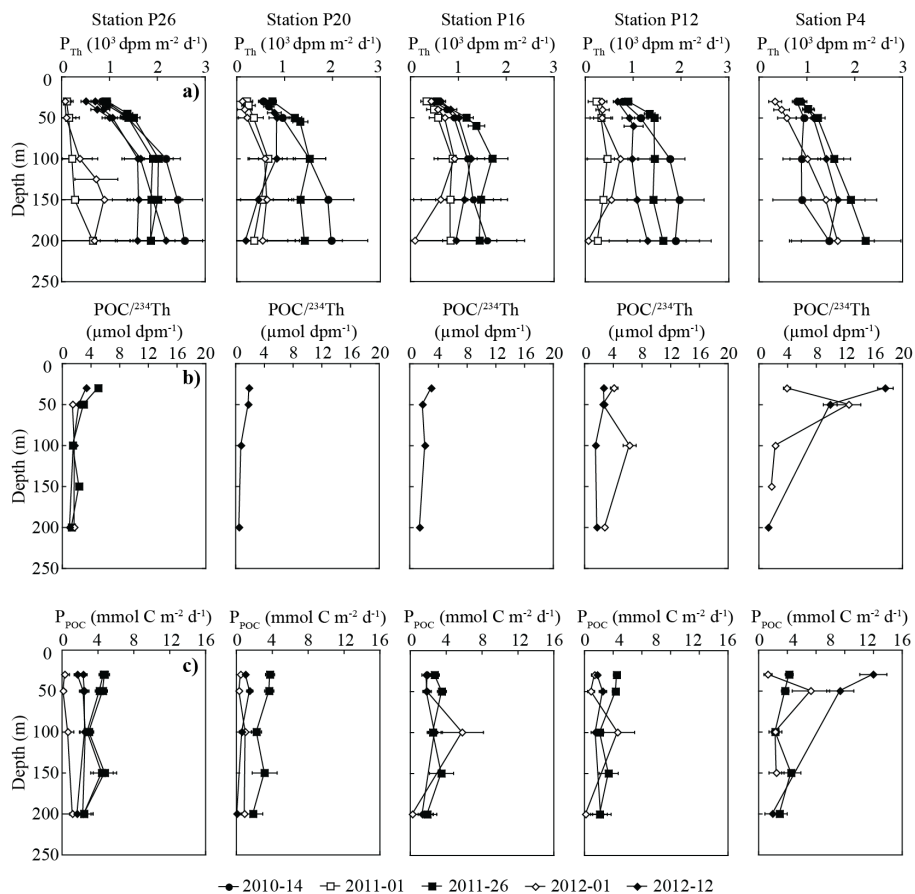


Fig. 9.

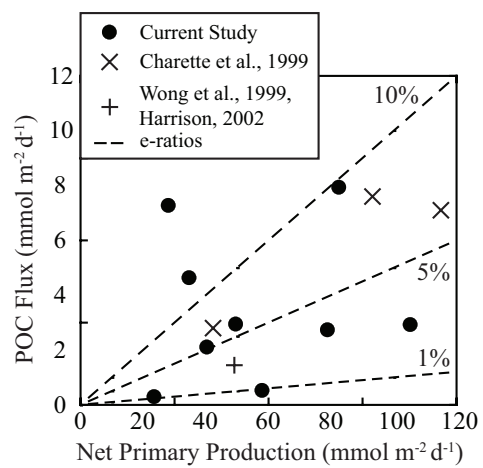


Fig. 10.

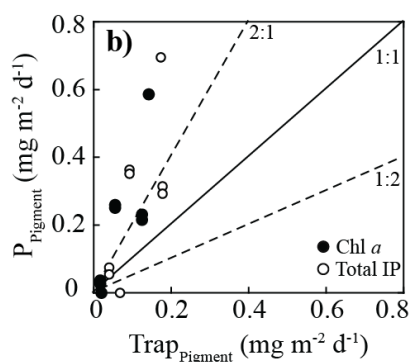
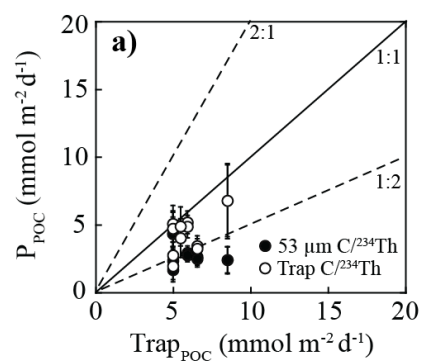


Fig. 11.

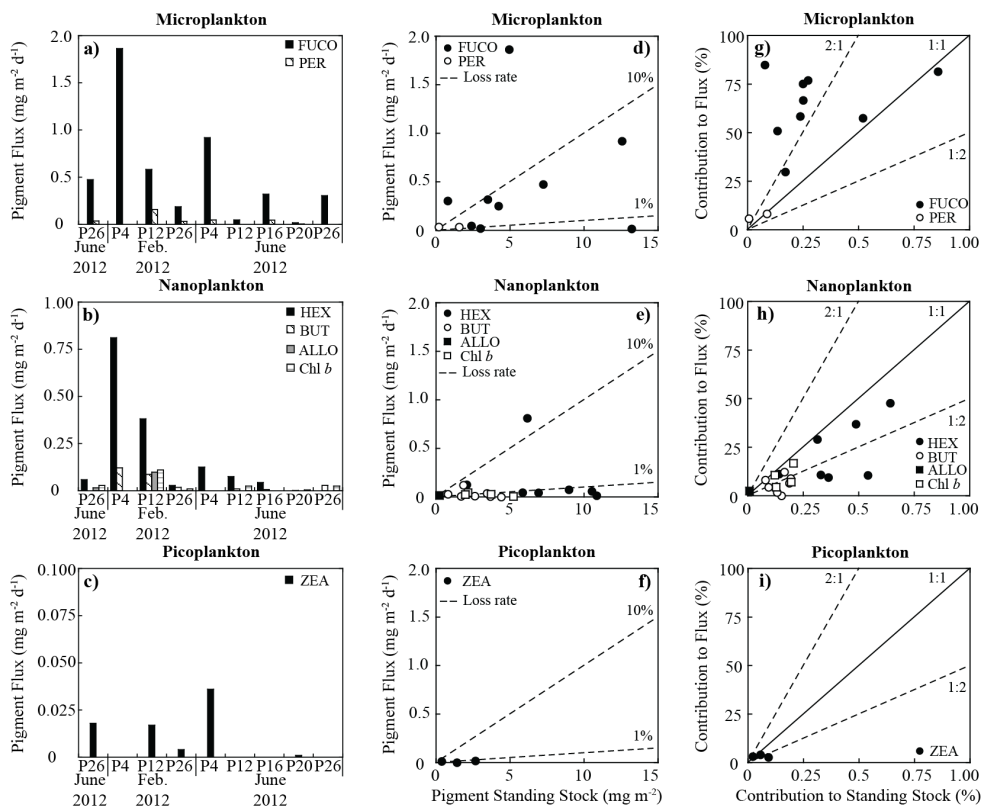


Fig. 12.